Investigation of the Concentration- and Temperature-Dependent Motion of Colloidal Nanoparticles

Barnaby Handel,[a] Vladislava Vladimirova,[a] Erving Ximendes,[a,b] José García Solé,[a] Daniel Jaque,[a,b]* Riccardo Marin[a]*

[a] Fluorescence Imaging Group (FIG), Departamento de Física de Materiales, Facultad de Ciencias, Universidad Autónoma de Madrid, C/ Francisco Tomás y Valiente 7, Madrid 28049, Spain.

[b] Nanobiology Group, Instituto Ramón y Cajal de Investigación, Sanitaria Hospital Ramón y Cajal, Ctra. De Colmenar Viejo, Km. 9100, 28034 Madrid, Spain.

ABSTRACT: Although the motion of a single nanoparticle suspended in a fluid can be easily modeled, things get complicated for non-infinitely diluted systems. Coincidentally, these latter are the systems of interest in relevant fields such as, nanomedicine, microfluidics and miniaturized energy storage devices. Hence, a better understanding of the dynamics of colloidal nanoparticles is utterly needed. Herein, the motion of colloidal suspension of plasmonic nanoparticles (i.e., gold nanoshells) is investigated via laser speckle imaging. The method relies on the analysis of the speckle pattern generated by colloidal suspensions forced to flow at specific velocities. Temperature-dependent measurements corroborated that the dynamics of non-infinitely diluted nanoparticle suspensions are better described through a diffusive model rather than by the equipartition theorem. Under the tested experimental conditions, an average diffusion velocity between 0.37 and 1.57 mm/s was found. Most importantly, these values were largely dependent on the nanoparticle concentration. These results are in agreement with previous reports and indicate the existence of long-range interactions between nanoparticles.

Introduction

As mundane as it might appear, the motion of particles suspended in a fluid is a subtle and intriguing investigation subject. It is not a coincidence that it constituted the topic of the doctoral thesis of one of the brightest minds of the last century: Albert Einstein.[1] However, investigations on the dynamics of colloidal nanoparticles are far from being spurred by a mere fundamental scientific curiosity. A better understanding of the motion of colloidal nanoparticles would ensure a more thorough comprehension of the thermal properties of nanofluids,[2] hence perfecting the control over heat exchange in next generation cooling and energy storage devices.[3, 4] The kinetics of colloidal nanoparticles in intracellular environments would also become interpretable, thus enabling investigations of biological processes that are at the base of life.[5]

The dynamics of a single nanoparticle in a liquid (*i.e.*, an ideal diluted suspension) are only governed by its interaction with the molecules of the dispersing medium (*vide infra*). The nanoparticle randomly changes its trajectory due to collisions with molecules of the liquid, ultimately resulting in what is referred to as Brownian motion. This is strictly true only in an infinitely diluted suspension, but reality is much more complex. Consider for instance that the long-term colloidal stability of a nanofluid is provided by the repulsive electrical forces between nanoparticles, which prevent precipitation and flocculation.[6, 7] In these conditions, nanoparticle dynamics result not only from the nanoparticle-molecule collisions, but also from interparticle interactions.

Optical tweezing is the method of choice to characterize the random motion of an isolated particle.[8] Using this approach, Kheifets and co-workers briefly observed the ballistic regime of the Brownian motion of dielectric microparticles, retrieving a velocity close to 0.2 mm/s, in good agreement with the value predicted by the

equipartition theorem.[9] However, this method does not allow to investigate the dynamics of suspended nanoparticles, as it does not consider the effect of interparticle interactions in nanofluids. Recently, Brites *et al.* addressed the subject of Brownian motion at the nanoscale.[10] In their study, the authors experimentally determined the velocity of sub-100 nm particles – ranging from 0.2 to 1.4 mm/s – through luminescence nanothermometry. They further demonstrated that nanoparticle velocity strongly depends on the nanofluid concentration revealing the presence of non-negigible interparticle interactions.

Inspired by these seminal results, we herein report on the use of laser-speckle contrast analysis (LASCA) to investigate the motion of plasmonic nanoparticles (i.e., gold nanoshells - GNSs) and the effect that particle concentration and temperature have on it. The method relies on the light scattering capabilities of the particles and it is hence applicable to a broad range of nanoparticles. We particularly focused our attention on plasmonic GNSs, due to their marked light scattering capability and the key role of plasmonic nanofluids in fields such as energy production, bio-sensing, microfluidics, pre-clinical imaging, field enhancement, and *in vivo* therapy.[11-16]

Theoretical background

Brief recall of the Brownian motion fundamentals

To discuss the obtained experimental results, it is useful to briefly recall the description of the Brownian motion of a suspended (nano)particle. Following the equipartition theory, the instantaneous velocity[17] acquired by a nanoparticle immediately after colliding with multiple solvent molecules, is given by:[18]

$$v_{NP,EQ} = \sqrt{\frac{3k_B T}{m^*}} \quad (1)$$

where k_B is the Boltzmann constant, T is the absolute temperature of the nanofluid, and m^* is the effective mass of the nanoparticle, *i.e.* the combined mass of the nanoparticle itself and the displaced fluid.[19] Equation (1) describes the ballistic regime, which is observed in the limit of very short timescales (roughly around 10^{-10} s in aqueous colloids).[10, 20] At longer times, a purely diffusive motion occurs, where the dynamics of the nanoparticle is determined by the drag force stemming from the solvent viscosity. In this diffusive regime, the velocity is given by the so-called Einstein-Stokes expression:[21]

$$v_{NP,ES} = \frac{2k_B T}{\pi \eta d_{NP}^2} \quad (2)$$

where η is the medium viscosity and d_{NP} is the diameter of the nanoparticle. Between the two "extreme" situations described by Equations (1) and (2), we find the hydrodynamic regime.[22] At that intermediate timescale, even in the limits of very low Reynolds numbers, a perturbed fluid flow field is generated in the vicinity of the nanoparticle.[23, 24] This is the result of momentum exchange between suspended nanoparticle and solvent molecules, which generates hydrodynamic memory in the fluid. The characteristic timescale of this regime is defined by the time required for the perturbed field to diffuse over a distance equal to the nanoparticle radius, and it depends on the viscosity and density of the fluid.[22]

Spatial speckle contrast

For the sake of the present study, we should regard a generic colloidal suspension of nanoparticles as an inhomogeneous system, where the homogeneous optical properties of the medium are locally perturbed by the presence of nanoparticles. Plasmonic nanoparticles could act as highly efficient scattering centres when illuminated with light falling within their plasmonic resonance band. The reflected image produced by a colloidal suspension of those particles follows a random pattern (laser speckle image) that arises from the interference of the scattered waves (Figure 1a and b).[25] The spatial speckle contrast (*K*) is defined as the ratio between the standard deviation (σ) and the average (I) of the light intensity measured over a specific kernel of pixels (here 5x5 – see Supporting Information).[26] In the ideal case of perfectly static scattering particles, the spatial speckle contrast is high, because of the large intensity variations between pixels (Figure 1c). When the particles are in motion, the laser speckle pattern becomes blurred, because of the fluctuating signals of the moving scattering centres. This leads to a more homogeneous pattern with a lower average intensity, which in turn results in lower spatial speckle contrast (Figure 1d). The relative change (reduction) in the speckle contrast is defined as the LASCA intensity (I_{LASCA}) in such a way that the lower the speckle contrast *K*, the higher the intensity of the LASCA image (see Supporting Information for details).[27]

LASCA takes advantage of this effect to provide 2D maps of the particle velocity (which is directly proportional to I_{LASCA}) by monitoring the change in contrast of the laser speckle image.

Given the above considerations, we propose that, for a fixed temperature, the LASCA

intensity generated by a nanofluid can be written as:

$$I_{LASCA} = \beta \cdot N \cdot v_{NP} \qquad (3)$$

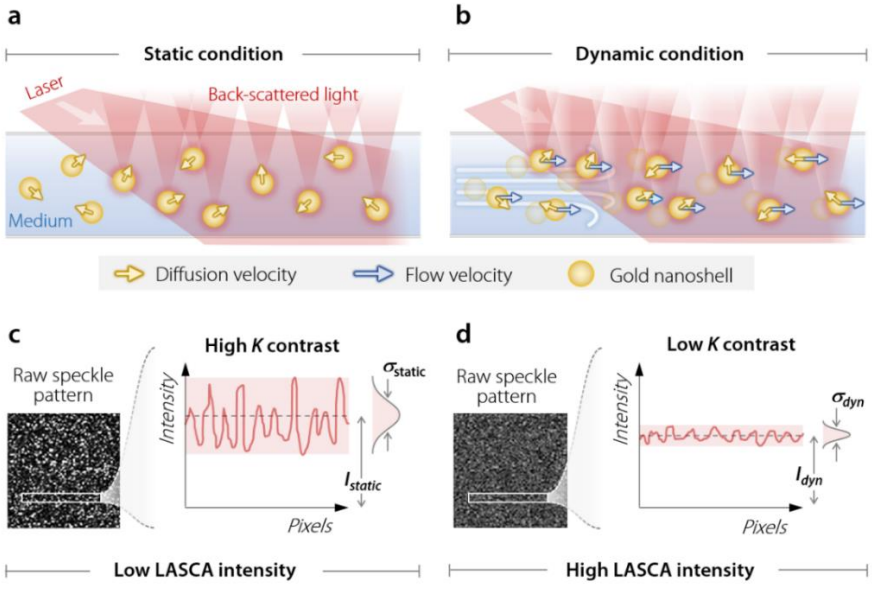

Figure 1. Schematic representation of the working principle of laser speckle imaging. **a** and **b)** depiction of a GNS nanofluid in a capillary in static and dynamic conditions, respectively, irradiated with a laser being scattered by the suspended nanoparticles. Yellow and blue arrows indicate the velocity resulting from random motion of the GNSs and an externally imposed flow velocity, respectively. **c** and **d)** corresponding speckle patterns obtained collecting the back-scattered light and variation of the back-scattered signal from the region of interest – indicated with a grey rectangle – in terms of standard deviation (⊠) and average intensity (*I*).

where β is a proportionality constant that depends on several parameters (including the response time of the optical system, the scattering cross section of colloidal nanoparticles, and the geometry of the observed system), N is the nanoparticle concentration (the linear relationship between N and I_{LASCA} is shown in Figure S1) and v_{NP} is the velocity of the colloidal nanoparticles. The direct proportionality between I_{LASCA} and v_{NP} directly stems from the way a LASCA image is produced (see Equations S1-S5 in the Supporting Information).

Results and discussion

LASCA measurements under an imposed flow

When dealing with a macroscopically static nanofluid, *i.e.*, a nanofluid that is not forced to flow, the static LASCA image intensity (I_{LASCA}^{st}) is given by:

$$I_{LASCA}^{st} = \beta \cdot N \cdot \langle v_{NP}^{st} \rangle (v_{diff}) \tag{4}$$

where $\langle v_{NP}^{st} \rangle$ is the average velocity of the suspended nanoparticles – a function of their diffusion velocity, *i.e.*, $\langle v_{NP}^{st} \rangle = \langle v_{NP}^{st} \rangle (v_{diff})$. The assumption of a purely diffusive regime is supported by the long integration time of the analysis (*i.e.*, 20 ms) and temperature-dependent measurements performed on the nanofluid (*vide infra*). When the fluid flows with a velocity v_f, the LASCA intensity is given by:

$$I_{LASCA}^{dyn} = \beta \cdot N \cdot \langle v_{NP}^{dyn} \rangle \left(v_f, v_{diff}\right) \tag{5}$$

where $\langle v_{NP}^{dyn} \rangle$ is the average velocity of the nanoparticles in these dynamic conditions. The diffusion velocity (v_{diff}) depends on the diffusivity (D) of the nanoparticle. Under an imposed flow, this parameter depends on the flow velocity.[28] However, in the same study, it was observed that D had no evident dependence on the flow velocity for nanoparticles that are large enough (*i.e.*, approx. 100 nm) and featuring cumbersome molecules at the surface. For this reason, in our study, we assumed that the diffusivity of the PEGylated GNS – and hence the magnitude of v_{diff} – is identical both in static and dynamic conditions.

The average velocity in static conditions can be derived mathematically (see Figure S2), and is equal to:

$$\langle v_{NP}^{st} \rangle = \frac{2}{\pi} v_{diff} \tag{6}$$

When an external flow is imposed, the total displacement of a nanoparticle during the observation time is larger, due to the additional contribution given by the flow velocity. In first approximation, we can simply consider the net velocity to be given by the sum of diffusion and flow velocities:

$$\langle v_{NP}^{dyn} \rangle = v_f + \frac{2}{\pi} v_{diff} \tag{7}$$

It follows that the ratio between the LASCA intensity measured in dynamic and static conditions can be written as:

$$I_{LASCA}^{norm} = \frac{I_{LASCA}^{dyn}}{I_{LASCA}^{st}} = \frac{\langle v_{NP}^{dyn} \rangle (v_f, v_{diff})}{\langle v_{NP}^{st} \rangle (v_{diff})} = 1 + \frac{\pi}{2} \frac{v_f}{v_{diff}} \quad (8)$$

It is thus possible to determine the diffusion velocity of colloidal nanoparticles from the analysis of a set of LASCA images of a nanofluids flowing at known v_f values. By considering the above ratio, any contribution played by the geometry of the observed system is eliminated – since the LASCA images acquired under static and dynamic conditions are equally affected by the geometry (see Figure S3 and S4).

The experimental set-up required for the determination of v_{diff} using LASCA is schematically shown in Figure 2a. A colloidal suspension of 240-nm-diameter GNSs (see Figure 2b for a TEM image of these nanoparticles) was placed inside a plastic tubing, then it was illuminated with a 785-nm laser and the speckle pattern registered and analyzed by a commercial laser speckle imaging system (MOORFLPI-2, Moor Instruments). The tubing was connected to a syringe pump, in order to externally impose different fluid velocities, v_f. The GNSs used in this study (total diameter = 240 nm, silica core diamter = 200 nm) were preferred over smaller (total diameter = 150 nm, silica core diamter = 120 nm) GNSs because of their stronger extinction at the laser wavelength, which yielded higher I_{LASCA} (Figure S5). The concentration of the GNSs was varied from $2.5 \cdot 10^8$ to $5 \cdot 10^9$ GNSs/mL, corresponding to volume fractions (ϕ) ranging from $3 \cdot 10^{-4}$ to $6.6 \cdot 10^{-3}$ %. These GNSs present a broad plasmonic band spanning from 500 to 1600 nm (Figure 2c), which encompasses the center wavelength of the laser used (785 nm), ensuring a high back-scattering signal level. During the measurements, the lack of appreciable temperature increase due to photothermal phenomena was checked with the aid of an infrared thermal camera. Four representative LASCA images, obtained for a GNS suspension (at a concentration of $5 \cdot 10^9$ GNS/mL; $\phi = 6 \cdot 10^{-3}$ %) under static and dynamic conditions, are shown in Figure 2d to 2g. A clear LASCA intensity enhancement was observed under dynamic conditions (flow velocity $v_f > 0$) compared to static conditions ($v_f = 0$). From the systematic acquisition of LASCA images obtained at different flow velocities, we obtained $I_{LASCA}^{norm}(v_f)$ vs v_f datasets

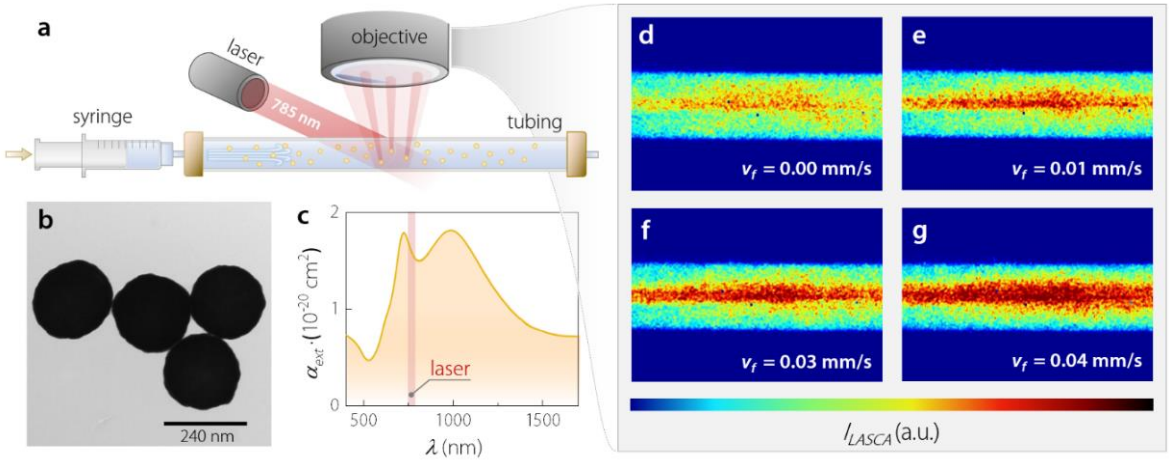

Figure 2. a) Schematic representation of the experimental set-up used for LASCA imaging of plasmonic nanofluids. **b)** TEM image of the 240-nm GNSs and **c)** their extinction spectrum in water suspension. The orange area indicates the wavelength range of the laser speckle instrument. **d-g)** LASCA images of a colloidal suspension of the GNSs ($\phi = 6.6 \cdot 10^{-3}$ %) without and with externally imposed flow.

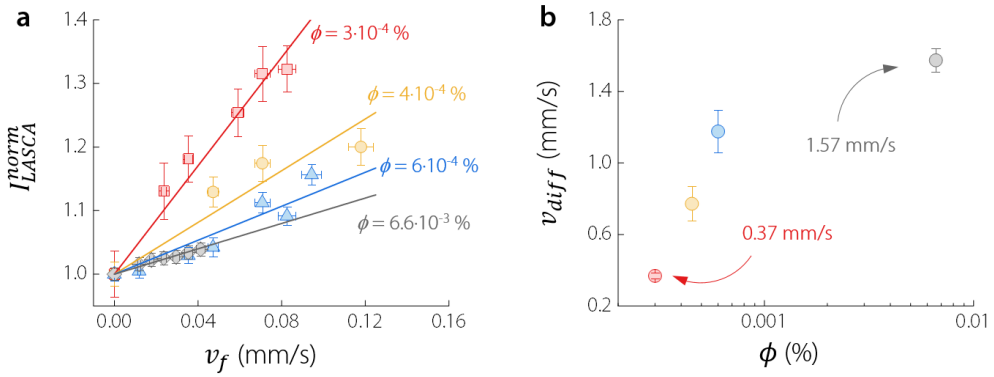

Figure 3. a) Normalized LASCA intensity vs flow velocity obtained for colloidal suspension of GNSs at different volume fractions. Solid lines are the fits according to Equation (8). R^2-values are all between 0.89 and 0.97. **b)** Diffusion velocity of GNSs obtained for different nanoparticle concentrations (measured in volume fraction, ☒). The velocity obtained for the most diluted sample that could be measured in our system was (0.37 ± 0.03) mm/s.

for different GNS concentrations (Figure 3a). For all the GNS concentrations used in this work, we found that $I^{norm}_{LASCA}(v_f)$ increases linearly with the flow velocity. It is important to note that for the highest concentration investigated in this work ($\phi = 6.6{\cdot}10^{-3}$ %) we obtained v_{diff} = (1.57 ± 0.07) mm/s, a value that decreased with decreasing GNS concentration. Indeed, for the most diluted sample that could be analyzed with our LASCA system ($\phi = 3{\cdot}10^{-4}$ %), the diffusion velocity of GNSs was found to be (0.37 ± 0.03) mm/s. These values are in agreement with the velocities experimentally determined for 23-nm upconverting nanoparticles in water (0.31-1.4 mm/s) by Brites *et al.*[10] (Table 1). Moreover, the correlation between v_{diff} and GNS concentration found in our work mirrors the trend observed between nanoparticle velocity and concentration in the above-mentioned study.[10]

Herein, this trend cannot be justified in light of a thermal conductivity change (as in Ref. 10), since our approach does not rely on the measurements of a thermal transient. Consequently, the effect of the concentration on the diffusion velocity must be instead explained as a result of interaction between nanoparticles. This interaction is likely two-fold in nature, entailing *i)* the vorticity of the fluid flow imparted by the motion of a moving nanoparticle,[29,30] which influences the motion of nearby nanoparticles, and *ii)* the electrostatic repulsion between nanoparticles, stemming from their surface charge needed for stability.[31] Both effects can act at longer range than an actual physical collision between nanoparticles – which can be ruled out due to the large distance between pairs of particles expected at the concentrations investigated here (Figure S6). Electrodynamic interactions should also be discarded, because of the use of an unfocused, low-power-density light source, which prevents optical binding phenomena to appear.[32]

Table 1 shows that the velocity determined at the lowest GNS concentration (0.37 mm/s) is almost two orders of magnitude smaller than the value calculated according to the equipartition theorem (v_{EQ} = 15 mm/s), but only roughly six times larger than the one predicted by the Einstein-Stokes model (v_{ES} = 0.06 mm/s). This observation supports the hypothesis that in our experimental conditions we are observing the diffusive regime of the nanofluid. The discrepancy with the value predicted by the Einstein-Stokes model likely arise from the fact that the interparticle interactions play a role even at the lowest tested

Table 1. Physical parameters and experimentally determined velocities of GNSs, $NaYF_4$ nanoparticles and $BaTiO_3$ microcrystals. The particle velocities predicted by the equipartition theorem and the Einstein-Stoke model are also included.

Particle	r (nm)	m (Kg)	m^* (Kg)	v_{exp} (mm/s)	v_{EQ} (mm/s)	v_{ES} (mm/s)	Reference
GNS	120	$4.8 \cdot 10^{-17}$	$5.1 \cdot 10^{-17}$	0.37	15	0.06	This work
$NaYF_4$	11	$2.7 \cdot 10^{-20}$	$3.1 \cdot 10^{-20}$	0.3	630	5.5	10
$BaTiO_3$	1860	$1.6 \cdot 10^{-13}$	$1.7 \cdot 10^{-13}$	0.18	0.26	0.0002	9

concentration. Indeed, by no means a volume fraction of $\phi = 3 \cdot 10^{-4}$ % represents the ideal case of an infinitely dilute system – *i.e.*, a single nanoparticle, which is the only case that the mathematical model can describe accurately. In stark contrast with out observation, the velocity reported for a single $BaTiO_3$ microparticle in acetone (0.18 mm/s), *i.e.*, of an infinitely diluted system, is in good agreement with the estimated Brownian velocity for the ballistic regime (0.26 mm/s) as predicted from the equipartition theorem.

Temperature-dependent experiment

To further support our data interpretation – *i.e.*, the observation of the diffusive regime via laser speckle imaging – we measured the temperature dependence of the measured GNS velocity. In the absence of any imposed flow, the LASCA intensity generated by a colloidal suspension of GNSs at room temperature (293 K, 20 °C) is given by:

$$I_{LASCA}^{st}(293\ \mathrm{K}) = \beta \cdot N \cdot v_{NP}(293\ \mathrm{K}) \tag{9}$$

where $v_{NP}(293\ \mathrm{K})$ is the velocity of nanoparticles suspended in the medium at room temperature.

When the solution is heated to a temperature T > 293 K, the LASCA intensity is given by:

$$I_{LASCA}^{st}(T) = \beta \cdot N \cdot v_{NP}(T) \tag{10}$$

where $v_{NP}(T)$ is the nanoparticle velocity at temperature *T*. . It is important to notice that β contains the scattering cross section of the GNSs, which is a paramter that depends on the tempeature, sue to changes in the permittivity of the medium. However, when passing from 293 to 333 K (the investigated temperature range), decreases of approximately 0.6 % (see Figure S7). For the sake of the present discussion, β can therefore be considered temperature-independent. Combination of Equations (9) and (10) allows to retrieve the temperature-induced relative increment of the nanoparticle velocity:

$$v_{NP}^{rel} = \frac{v_{NP}(T)}{v_{NP}(293\ \mathrm{K})} = \frac{I_{LASCA}^{st}(T)}{I_{LASCA}^{st}(293\ \mathrm{K})} \tag{11}$$

According to Equation (11), the acquisition of LASCA images of a static GNS colloid at different temperatures can be used to elucidate the temperature dependence of the nanoparticle velocity. In Figure 4a, three representative LASCA images of a static colloidal solution of GNSs obtained at different temperatures are reported. Evidently LASCA intensity increases with temperature. Indeed, Figure 4b shows that LASCA intensity – and hence the relative nanoparticle velocity – at 333 K is approximately twice as high compared to room temperature. A monotonous increment of the LASCA intensity ratio of a colloidal suspension of GNSs (0.01 % volume fraction) with the temperature is observed (grey dots). These experimental data can be compared to the theoretical predictions made on the basis of Equations (1) and (2). The temperature dependence of the nanoparticle velocity according to the equipartition ($v_{NP,EQ}^{rel}$) and the Einstein-Stoke ($v_{NP,ES}^{rel}$) models are respectively given by:

$$v_{NP,EQ}^{rel} = \sqrt{\frac{T}{293}} \tag{12}$$

$$v_{NP,ES}^{rel} = \frac{T \cdot \eta_{RT}}{293 \cdot \eta\ (T)} \tag{13}$$

where T is the absolute temperature of the suspension, η_{RT} is the water viscosity at room temperature (293 K) and $\eta\ (T)$ is the water viscosity at absolute temperature T.

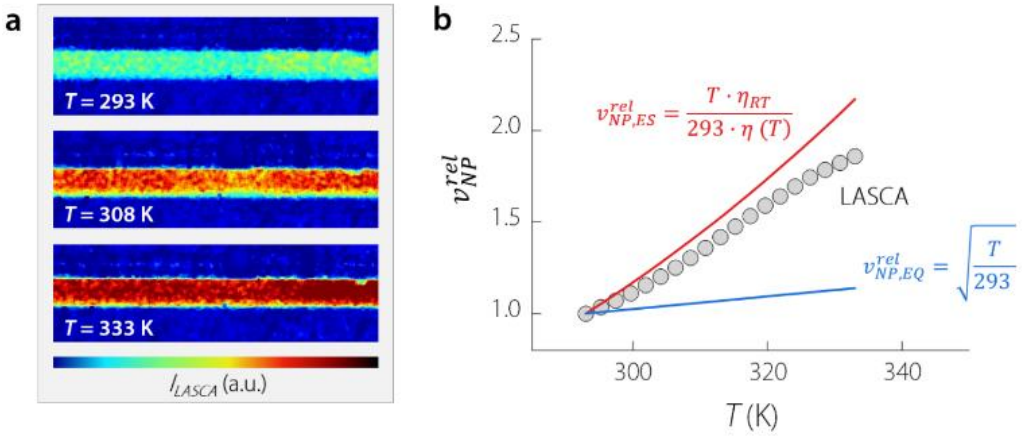

Figure 4. a) LASCA images of a colloidal suspension of GNSs (☒ = 0.01 %) in absence of imposed flow velocity (static conditions) obtained at different temperatures. **b)** Temperature dependence of the normalized LASCA intensity obtained from the analysis of the images obtained at different temperatures. Grey circles are experimental data and solid lines represent the theoretical predictions.

Note that, in the temperature range here analyzed (293-333 K), the equipartition theorem predicts an almost negligible change in the nanoparticle velocity (solid blue line in Figure 4b). On the other hand, the Einstein-Stokes model predicts a more marked temperature-induced increment. Evidently, the latter model gives a better description of the experimental data. Therein, the temperature-induced increment of the nanoparticle velocity is prompted by the strong temperature dependence of the water viscosity that decreases from $1 \cdot 10^{-3}$ (293 K) to $0.46 \cdot 10^{-3}$ Pa s (333 K).[33] Hence, a 13-% increment in absolute temperature leads to a reduction in water viscosity greater than 50 %, which is consistent with the observed almost two-fold nanoparticle velocity increase.

Conclusions

In summary, we demonstrated the use of a laser-speckle-based technique to investigate the dynamics of scattering (plasmonic) nanofluids. The proposed experimental approach is based on a straightforward analysis of the speckle patterns generated by colloidal dispersions of nanoparticles both in static conditions and under an applied flow. This method was applied to determine the diffusion velocity of colloidal gold nanoshells in water and its dependence on the nanofluid concentration. The increase of the diffusion velocity with the nanoparticle concentration was attributed to long-range interactions between the suspended gold nanoshells – namely, hydrodynamic and electrostatic – rather than to collisions between them. For the most diluted sample, the diffusion velocity was 0.37 mm/s. Both the magnitude and the concentration-dependent nature of the reported nanoparticle velocity are in agreement with previous results obtained using an experimental approach based on luminescence thermometry. Additional experiments were conducted varying the temperature of the nanofluid, observing an increase of the nanoparticle velocity with the temperature of the colloidal dispersion.

Overall, comparison of the experimental results with the predictions based on the equipartition theorem and the Einstein-Stokes model afforded three main conclusions: i) the proposed laser-speckle technique allows observing the diffusion regime of the colloidal dispersion – rather than its ballistic regime, ii) the dynamics of the nanofluids are greatly influenced by the temperature-dependent viscosity of the medium, iii) even in highly diluted dispersions, the dynamics of nanofluids are governed by (long-distance) interactions between suspended nanoparticles.

Conflicts of interest

There are no conflicts to declare.

Acknowledgements

This project was partially funded by the European Commission through the European Union's Horizon 2020 research and innovation program under the Marie Skłodowska-Curie Grant agreement No. 797945 "LANTERNS", by the Spanish Ministry of Economy and Competitiveness under project MAT2016-75362-C3-1-R, and by the Comunidad Autónoma de Madrid (B2017/BMD-3867RENIMCM), and co-financed by the European Structural and investment fund. Additional funding was provided by the European Union's Horizon 2020 FET Open programme (grant agreement No 801305), the Fundacion para la Investigación Biomédica del Hospital Universitario Ramon y Cajal project IMP18_38 (2018/0265).

References

1. A. Einstein, *Ann. Phys.*, 1905, **322**, 549-560.

2. A. Gupta and R. Kumar, *Appl. Phys. Lett.*, 2007, **91**, 223102.

3. A. H. Elsheikh, S. W. Sharshir, M. E. Mostafa, F. A. Essa and M. K. Ahmed Ali, *Renew. Sust. Energy Rev.*, 2018, **82**, 3483-3502.

4. A. Kasaeian, A. T. Eshghi and M. Sameti, *Renew. Sust. Energy Rev.*, 2015, **43**, 584-598.

5. C. Di Rienzo, V. Piazza, E. Gratton, F. Beltram and F. Cardarelli, *Nat. Commun.*, 2014, **5**, 5891.

6. X. Xing, G. Sun, Z. Li and T. Ngai, *Langmuir*, 2012, **28**, 16022-16028.

7. J. Mewis and N. J. Wagner, *Colloidal suspension rheology*, Cambridge University Press, 2011.

8. K. Dholakia, P. Reece and M. Gu, *Chem. Soc. Rev.*, 2008, **37**, 42-55.

9. S. Kheifets, A. Simha, K. Melin, T. Li and M. G. Raizen, *Science*, 2014, **343**, 1493-1496.

10. C. D. Brites, X. Xie, M. L. Debasu, X. Qin, R. Chen, W. Huang, J. Rocha, X. Liu and L. D. Carlos, *Nat. Nanotechnol.*, 2016, **11**, 851-856.

11. A. R. Mallah, M. N. Mohd Zubir, O. A. Alawi, K. M. Salim Newaz and A. B. Mohamad Badry, *Solar Energy Mater. Solar Cells*, 2019, **201**, 110084.

12. J. Kim, *Lab Chip*, 2012, **12**, 3611-3623.

13. A. R. Rastinehad, H. Anastos, E. Wajswol, J. S. Winoker, J. P. Sfakianos, S. K. Doppalapudi, M. R. Carrick, C. J. Knauer, B. Taouli, S. C. Lewis, A. K. Tewari, J. A. Schwartz, S. E. Canfield, A. K. George, J. L. West and N. J. Halas, *Proc. Natl. Acad. Sci.*, 2019, **116**, 18590-18596.

14. R. A. Alvarez-Puebla, A. Agarwal, P. Manna, B. P. Khanal, P. Aldeanueva-Potel, E. Carbo-Argibay, N. Pazos-Perez, L. Vigderman, E. R. Zubarev, N. A. Kotov and L. M. Liz-Marzan, *Proc. Natl. Acad. Sci.*, 2011, **108**, 8157-8161.

15. M. S. Strozyk, M. Chanana, I. Pastoriza-Santos, J. Pérez-Juste and L. M. Liz-Marzán, *Adv. Funct. Mater.*, 2012, **22**, 1436-1444.

16. J. Hu, F. Sanz-Rodríguez, F. Rivero, E. M. Rodríguez, R. A. Torres, D. H. Ortgies, J. G. Solé, F. Alfonso and D. Jaque, *Nano Res.*, 2017, **11**, 676-685.

17. A. Einstein, *Z. Elektrochem. Angew. Physik. Chem.*, 1907, **13**, 41-42.

18. R. E. Burgess, *Phys. Lett. A*, 1973, **42**, 395-396.

19. R. Zwanzig and M. Bixon, *J. Fluid Mech.*, 2006, **69**, 21-25.

20. R. Huang, I. Chavez, K. M. Taute, B. Lukić, S. Jeney, M. G. Raizen and E.-L. Florin, *Nature Phys.*, 2011, **7**, 576-580.

21. D. H. Kumar, H. E. Patel, V. R. Kumar, T. Sundararajan, T. Pradeep and S. K. Das, *Phys. Rev. Lett.*, 2004, **93**, 144301.

22. T. Franosch, M. Grimm, M. Belushkin, F. M. Mor, G. Foffi, L. Forro and S. Jeney, *Nature*, 2011, **478**, 85-88.

23. G. L. Paul and P. N. Pusey, *J. Phys. A: Math. Gen.*, 1981, **14**, 3301-3327.

24. R. F. Fox, *J. Math. Phys.*, 1977, **18**, 2331-2335.

25. J. D. Briers and S. Webster, *J. Biomed. Opt.*, 1996, **1**, 174-179.

26. D. A. Boas and A. K. Dunn, *J. Biomed. Opt.*, 2010, **15**, 011109.

27. A. F. Fercher and J. D. Briers, *Opt. Commun.*, 1981, **37**, 326-330.

28. K. Katayama, H. Nomura, H. Ogata and T. Eitoku, *Phys. Chem. Chem. Phys.*, 2009, **11**, 10494-10499.

29. F. M. Mor, A. Sienkiewicz, L. Forró and S. Jeney, *ACS Photonics*, 2014, **1**, 1251-1257.

30. B. J. Alder and T. E. Wainwright, *Phys. Rev. Lett.*, 1967, **18**, 988-990.

31. F. Giorgi, D. Coglitore, J. M. Curran, D. Gilliland, P. Macko, M. Whelan, A. Worth and E. A. Patterson, *Sci Rep*, 2019, **9**, 12689.

32. F. Nan, F. Han, N. F. Scherer and Z. Yan, *Adv Mater*, 2018, **30**, e1803238.

33. L. Korson, W. Drost-Hansen and F. J. Millero, *J. Phys. Chem.*, 1969, **73**, 34-39.